

Contactless calibration of microchanneled AFM cantilevers for fluidic force microscopy

Sebastian Sittl  | Nicolas Helfricht  | Georg Papastavrou 

Department of Chemistry II, University of Bayreuth, Bayreuth, Germany

Correspondence

Georg Papastavrou, Department of Chemistry II, University of Bayreuth, Universitätsstr. 30, Bayreuth, Germany.
Email:
georg.papastavrou@uni-bayreuth.de

Funding information

Deutsche Forschungsgemeinschaft, Grant/Award Numbers: 391977956-SFB 1357/B01, 491183248

Abstract

Atomic force microscopy (AFM) is an analytical technique that is increasingly utilized to determine interaction forces on the colloidal and cellular level. Fluidic force microscopy, also called FluidFM, became a vital tool for biomedical applications. FluidFM combines AFM and nanofluidics by means of a microchanneled cantilever that bears an aperture instead of a tip at its end. Thereby, single colloids or cells can be aspirated and immobilized to the cantilever, for example, to determine adhesion forces. To allow for quantitative measurements, the so-called (inverse) optical lever sensitivity (OLS and InvOLS, respectively) must be determined, which is typically done in a separate set of measurements on a hard, non-deformable substrate. Here, we present a different approach that is entirely based on hydrodynamic principles and does make use of the internal microfluidic channel of a FluidFM-cantilever and an external pressure control. Thereby, a contact-free calibration of the (inverse) optical lever sensitivity (InvOLS) becomes possible in under a minute. A quantitative model based on the thrust equation, which is well-known in avionics, and finite element simulations, is provided to describe the deflection of the cantilever as a function of the externally applied pressure. A comparison between the classical and the here-presented hydrodynamic method demonstrates equal accuracy.

KEYWORDS

atomic force microscopy, bio(adhesion), fluidic force microscopy, instrumentation, method development, nanomanipulation

1 | INTRODUCTION

Atomic force microscopy (AFM) established itself as a powerful analytical technique with applications in biomaterials, cell biology, surface coatings, and colloid science.^{1–7} Originally, AFM has been developed to image the topography of a sample, also in liquid environment.¹ However,

AFM plays an increasingly important role in quantitatively determining interaction and adhesion forces.^{2,8} AFM is sensitive enough to detect forces on the single colloid^{9–11} or single cell level.^{12,13} For such direct force measurements, an AFM-cantilever can be modified by replacing the sharp tip, which is commonly used for imaging, with a colloidal particle,^{9,10} a hydrogel bead,¹⁴ or a cell.^{12,13} The

This is an open access article under the terms of the [Creative Commons Attribution](https://creativecommons.org/licenses/by/4.0/) License, which permits use, distribution and reproduction in any medium, provided the original work is properly cited.

© 2023 The Authors. *VIEW* published by Shanghai Fuji Technology Consulting Co., Ltd, authorized by Professional Community of Experimental Medicine, National Association of Health Industry and Enterprise Management (PCEM) and John Wiley & Sons Australia, Ltd.

development of fluidic force microscopy originated less than 15 years ago.¹⁵ This technique proved to be very versatile and allowed for reversibly formed colloidal probes^{16–18} and the aspiration of sessile cells on a substrate, which allows for quantitative characterization of their detachment forces.^{19–23} For biological applications, fluidic force microscopy is not limited to the determination of adhesion forces of cells on various substrates. Currently, intracellular injection or sampling of organelles under precise force control are actively pursued by this technique.^{20,24} However, these applications require an even more precise control of the acting forces.²⁵

To determine quantitative interaction forces by AFM, various elements of the experimental setup must be calibrated, including the spring constant of the AFM cantilever utilized and the sensitivity of the optical lever detection arrangement. Various calibration methods for the cantilever's spring constant have been established in the last 30 years.^{26–29} It is generally accepted that an accuracy of 5%–10% for the spring constant can be routinely achieved.^{30,31} Interestingly, the calibration of the optical lever detection system received considerably less attention in the literature, albeit equally important for the accuracy of the experimentally determined interaction forces.^{32,33} The so-called “optical lever technique” traces the deflection of the cantilever by following the position change of a laser beam that is reflected at the end of the cantilever onto a quadrant photodiode or position-sensitive device.³⁴ This detection technique is very simple to implement and is currently representing the quasi-standard in commercial instruments, as it is capable of detecting forces in the low pico-Newton regime in combination with sufficiently soft cantilevers.³⁵ The standard procedure for determining the inverse optical lever sensitivity, that is the proportionality factor between cantilever deflection (typically in nanometer) and resulting voltage change as recorded by the position-sensitive device, in the following abbreviated as InvOLS, is straightforward. It is based on acquiring the sensor voltage as a function of the *z*-piezo displacement, while the cantilever is pressed onto a non-deformable substrate. Interestingly, the original procedure^{2,36} has not changed significantly since the first presentation of the optical lever technique in the late 1980s.³⁴ Calibrating the optical lever sensitivity must be performed at precisely the same conditions (refractive index of solvent, position of the laser spot, etc.) under which the force profiles will be or have been measured. The nearly ubiquitous presence of thermal shifts in the experimental setup, partly due to the illumination with the laser, requires frequent repetitions and validation of the InvOLS-calibration.³⁷

Most biological samples are soft and thus are not suitable as substrates for the “classical” calibration of InvOLS. Thus, calibration must be directly carried out on the sub-

strate, such as petri dishes,³² or additional surfaces, such as glass slides, must be added to the fluid cell. Refined protocols require time and contact with a solid surface.³⁸

In the past, some contact-free approaches for the calibration of the (inverse) optical lever sensitivity have been reported. Unfortunately, these require additional, sophisticated equipment, such as optical tweezers, which are not easy to implement as the cantilever must be positioned on a special structure with high accuracy.^{39,40} Another, example would be the acquisition of the thermal noise spectrum of a cantilever whose spring constant is known from independent measurements.³³ However, in liquid, the accuracy of this approach is limited due to the substantial hydrodynamic damping, and thus low *Q*-factor for soft cantilevers. Other approaches rely on fast vertical movements of the cantilever in a viscous liquid to extract from the hydrodynamic drag and the top-view dimensions of the optical lever sensitivity.⁴¹

Here, we present a new approach to calibrate the (inverse) optical lever sensitivity for cantilevers used in fluidic force microscopy. These FluidFM-cantilevers have an internal microchannel and are mostly used for the study of biological samples. Hence, the before-mentioned limitations with respect to the calibration of the optical lever sensitivity by the classical method are most valid. The here-developed technique is based on the recoil experienced by the lever when a liquid jet is ejected from the cantilever's aperture by applying a defined external pressure to the microchannel. The here-presented novel method has several advantages: First, it is very fast to perform and can be easily integrated into automated workflows for high-throughput measurements. Secondly, no additional substrate is required as the method is entirely contact-free. Hence, it will be of great practical relevance for this increasingly utilized class of AFM cantilevers, especially in biological applications. It has been reported that an insufficiently calibrated optical lever sensitivity can introduce errors of 30% to determined forces.³² Moreover, high-throughput approaches based on the FluidFM technique based on robotic setups would greatly profit from a fast and contact-free calibration of the optical lever technique.^{21,42,43}

Comprehensive introductions to the optical lever method and fluidic force microscopy are given below, as both are relevant for the here-presented method of InvOLS calibration.

1.1 | Optical lever sensitivity

The schematic inset in Figure 1A illustrates the optical lever method as utilized in most AFMs.³⁴ The beam of a non-coherent laser diode is reflected at the backside of the

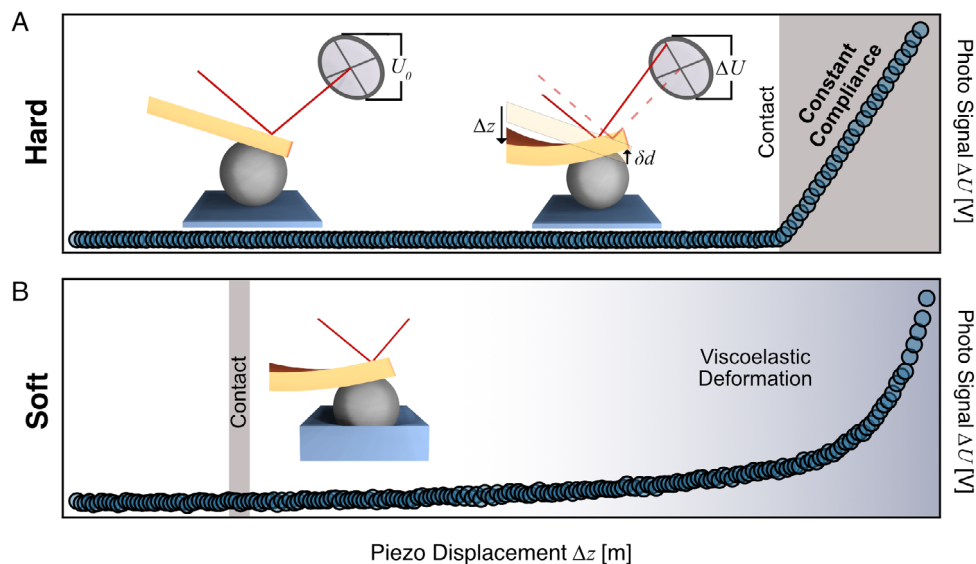


FIGURE 1 (A) Schematic representation of the optical lever detection for the deflection δd of a cantilever in an AFM. Approaching the cantilever towards the surface by moving the piezo stage for Δz , the resulting deflection δd is acquired by the shift of the reflected laser spot on a position-sensitive detector. This shift leads to a difference in the output potential ΔU of the detector. (A) The interaction for a hard substrate: Upon contact, the piezo-travel Δz corresponds to an equal deflection δd (constant compliance regime). (B) By contrast, the interaction with a soft substrate includes viscoelastic deformation of the sample. The applied force during piezo displacement leads to a deformation of the sample besides the deflection of the cantilever.

cantilever to a position-sensitive photodetector. Deflection of the lever δd leads to a change of ΔU in the readout of the photodiode as the position of the laser spot on the detector changes (cf. the inset in the middle of Figure 1A). For sufficiently small deflections, the proportionality $\delta d \propto \Delta U$ can be postulated, and the following Equation (1) can be written:

$$\text{InvOLS} = \delta d / \Delta U \quad (1)$$

where InvOLS is the inverse optical lever sensitivity. By Hooke's law, the deflection δd corresponds to the force F acting on the cantilever by

$$F = k_c \cdot \delta d \quad (2)$$

where k_c is the spring constant of the cantilever.

The sensitivity of the optical lever detection, expressed by the quantity InvOLS, is directly traceable from the cantilever response in the so-called constant compliance region. In contact, any movement of the z -piezo by Δz leads directly to a resulting deflection δd of the cantilever (cf. Figure 1A). A linear fit of the constant compliant regime gives the InvOLS according to Equation (1). InvOLS is of central importance for the optical lever technique.^{34,44,45} It is required for converting the raw data from direct force measurements (i.e., photodetector voltage vs. z -piezo displacement) to force profiles (i.e., force vs. distance).^{2,36} Moreover, the deflection of the cantilever has to be taken

into account to calculate the true separation distance from the raw piezo-displacement (cf. Figure 1).^{2,36} Hence, any measurement errors in determining the InvOLS do not only influence the forces reported, but also the distances of the resulting force profiles.

However, a prerequisite for the presented 'classical' calibration method is that the sample is non-deformable, which is strictly valid only for surfaces, such as sapphire, silicon wafers, or glass.^{34,36} In the case of soft surfaces or films that show viscoelastic behavior, the response upon contact and exertion of a force is non-linear. A schematic example of the photodetector signal versus piezo-displacement encountered on such a surface is shown in Figure 1B. Typical examples for such surfaces are biological tissues and cells^{46,47} or polymer coatings on solid substrates.⁴⁸ Practically, almost all surfaces relevant to biomedical studies must be considered soft. Hence, the calibration of InvOLS has to take place in separate measurements or by placing additional non-deformable substrates in the measurement cell of the AFM.⁴⁹ It is also important to stress that the path of the light beam and the position of the laser spot must be exactly the same for the calibration as for actual measurements.^{49,50} Hence, it is impossible to determine the optical lever sensitivity a posteriori under ambient conditions if the actual measurements have been carried out, for example, in a buffer solution.⁵¹ Moreover, in the case of colloidal probes, the mechanical law of leverage must be considered for quantitative measurements. Hence, InvOLS-calibration for a

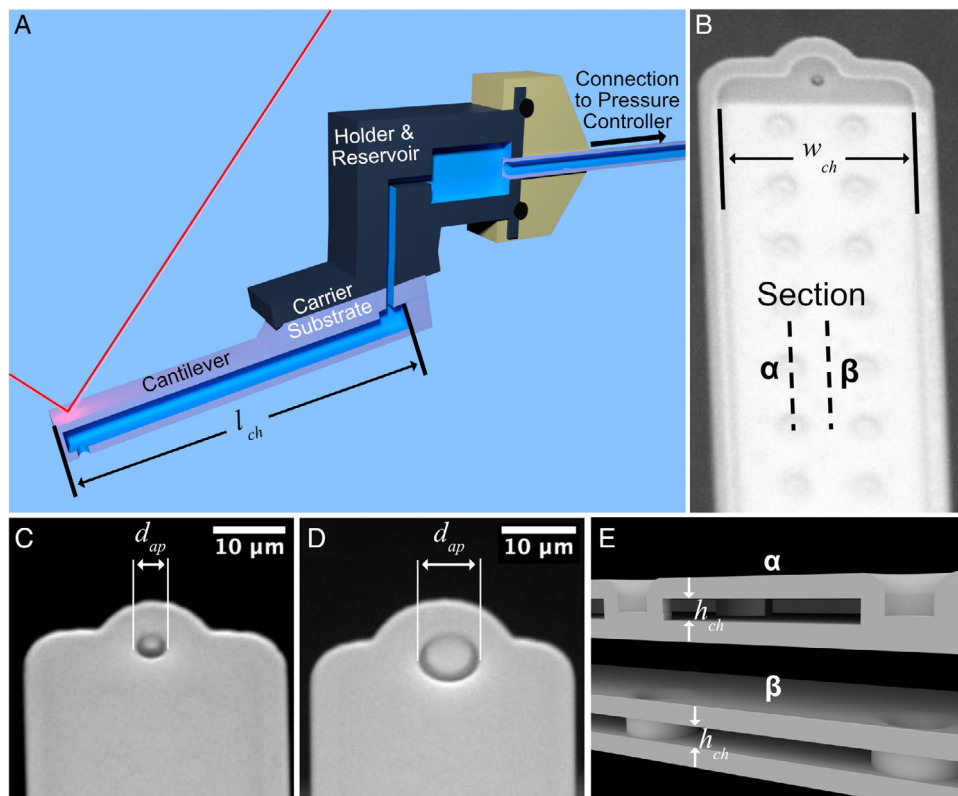


FIGURE 2 Schematic representation of a typical fluidic force microscopy setup, which includes a microchanneled cantilever and its support structure (reservoir, connector, and tubing) as well as a pressure controller (not shown). The cantilever is filled with electrolyte solution and immersed in a liquid cell. The internal channel extends into the supporting chip and is longer than the lever arm. The total length l_{ch} of the internal channel is 1.4 mm. (B) SEM image of a microchanneled AFM cantilever bearing a $2\text{-}\mu\text{m}$ aperture (in diameter) at its free end. The round structures within the channel structure are pillars supporting the sandwiched structure. (C and D) SEM images of apertures with nominal diameters d_{ap} of 4 and $8\text{ }\mu\text{m}$, respectively. (E) Schematic representations of cross-sections through a microchanneled cantilever illustrating the channel height h_{ch} and the pillars within the channel (α : cross-section through a pillar structure, β : cross-section through the free path of the channel), respectively.

tipless cantilever is different compared to a cantilever with an attached colloid.⁵²

1.2 | Fluidic force microscopy

Fluidic force microscopy, also referred to as FluidFM, is based on a standard AFM setup,¹⁵ including the use of the optical lever technique to determine the deflection of the cantilever.³⁴ The significant difference to standard AFM is that the cantilevers for FluidFM have an internal microchannel that ends in an aperture at the end of the cantilever. These cantilevers are connected via a reservoir and tubing to a pressure controller comparable to those used for microfluidics. Figure 2A shows a schematic representation of the essential components as required for fluidic force microscopy. By varying the externally applied pressure, fluid can be aspirated and ejected via the aperture of the cantilever.¹⁵ Thereby, various types of experimental procedures can be implemented for applications in cell biology,^{25,53–57} colloidal science,^{16–18} the structuring of

hydrogels and interfaces,^{58,59} scanning ion conductance microscopy (SICM),^{60,61} and the deposition of metals and colloidal particles.^{62,63} The internal flow of liquid in the cantilever can be followed by particle image tracking⁶⁴ or by streaming potential measurements.⁶⁵

Cantilevers with an internal microchannel for fluidic force microscopy are commercially available and have also been purposely constructed.^{66–69} To allow for an internal channel, commonly, a sandwich type of structure is chosen.^{70–72} Most studies rely on commercially available cantilevers from one company (Cytosurge) that differ only in the two parameters: aperture diameter and channel height. Scanning electron microscopy (SEM) images illustrating the features of these cantilevers, known as Micropipette cantilevers, are shown in Figure 2B–D. The regularly distributed round structures along the cantilever beam, visible in Figure 2B, are pillars supporting the sandwich structure. Figure 2E shows in a schematic manner the structural cross-section of the microchannel in the cantilevers used in this study. The sections α and β represent two different positions for the cross-section.

Important parameters for the microfluidic behavior within a FluidFM-cantilever are the internal height of the channel h_{ch} and its cross-sectional area A_{ch} . Figure 2C,D shows SEM images of FluidFM cantilevers with two different nominal aperture diameters d_{ap} (4 and 8 μm , respectively). The commercially available diameters range from 300 nm to 8 μm . It should be noted that the channel height also influences the spring constant of the sandwiched cantilever structure.^{73,74}

2 | RESULTS

First, the validity of the underlying physical models will be evaluated by experiments and simulations. Then, two experimental procedures will be presented for the hydrodynamic evaluation of InvOLS. Finally, we evaluated the accuracy of the newly developed method by comparison to the classical technique, where the cantilever is ramped against a hard surface.

2.1 | Recoil of a microchanneled cantilever upon fluid ejection

In fluidic force microscopy experiments, the fluid is commonly aspirated into the aperture of a microchanneled cantilever, either to immobilize colloidal particles on the cantilever or to aspirate and subsequently detach cells from a surface.^{25,54,55} However, a few experimental approaches make use of the possibility to eject fluid through the aperture to structure hydrogels,⁵⁸ deposit nanoparticles,⁷⁵ or to print 3D metal structures.⁶² Commonly, the pressure range exerted in such fluidic force microscopy experiments falls in the range of 20 mbar up to 1 bar.⁷⁵

An analogous situation to the ejection of liquid out of the cantilever's aperture is given by the gas ejection from the nozzle of a rocket, as shown schematically in Figure 3A. According to Newton's third law (*actio = reactio*), the expulsion of a mass Δm does lead to a force in the opposite direction.⁷⁶ As a rocket is pushed forward by the ejected jet of gas, the same applies to the ejected liquid from the cantilever's aperture. The resulting recoil force F_{rec} does lead to the cantilever bending upwards, as shown schematically in Figure 3B. It should be noted that in the situation outlined in Figure 3B, the cantilever is completely immersed in the same fluid, here water or an electrolyte solution, as the liquid ejected through the aperture. In principle, also recoil by pressing gas through the microchannel can be generated under ambient atmospheric conditions (i.e., in air). However, due to the fact that gas does not behave analogous to an incompressible Newtonian fluid, the quantitative analysis would be dif-

ferent from the one described below. In the case of two different phases, such as gas ejected in a liquid environment, surface tension would dominate the process due to the small dimensions involved.

Rocket propulsion has been studied in considerable detail in the past century. The so-called general thrust equation provides an adequate description not only for rockets but also for the here-presented microchanneled cantilevers.⁷⁶ By replacing the nozzle of a rocket with the aperture a FluidFM-cantilever, one obtains⁷⁶

$$F_{\text{rec}} = \frac{dm}{dt} \cdot v_{\text{ap}} + \Delta p \cdot A_{\text{ap}} \quad (3)$$

Here, dm/dt is the mass flow rate, v_{ap} the velocity of the liquid jet leaving the aperture with an area A_{ap} . Moreover, Δp is the pressure difference between the pressure inside the aperture and the pressure in the surrounding medium. For fluidic force experiments in the liquid phase, the externally applied pressure p_{ext} , which is the pressure applied via the microfluidic pressure controller, does not correspond directly to Δp . According to the law of Hagen–Poiseuille, the internal channel structure, as well as the friction of the liquid at the internal channel walls, lead to a significant pressure reduction (cf. Figure S5).⁷⁷ However, the effective pressure difference at the aperture is approximately proportional to the externally applied pressure: $\Delta p \propto p_{\text{ext}}$. According to the law of Bernoulli, the same is valid for the first term in Equation (3): $dm/dt \cdot v_{\text{ap}} \propto p_{\text{ext}}$.⁷⁸ Hence, hydrodynamics postulates a direct proportionality between recoil force and externally applied pressure $F_{\text{rec}} \propto p_{\text{ext}}$.

Figure 3C,D summarizes the results for experiments in which the deflection has been measured as function of externally applied pressure. Figure 3C shows deflection versus distance profiles as acquired at externally applied pressures ranging from -800 mbar to $+1000$ mbar in discrete steps. For each pressure step, p_{ext} was kept constant for the entire deflection versus distance profile. For each curve of Figure 3C, the deflection of the cantilever has been acquired in function of the displacement Δz of the z -piezo, while the external pressure remained constant. To obtain quantitative deflection data, the InvOLS has been calibrated beforehand on a non-deformable substrate by the “classical” method outlined previously at $p_{\text{ext}} = 0$ mbar. To convert Δz , the piezo-travel, to the separation distance D_i between the sample and the cantilever's aperture, the deflection of the cantilever must be taken into account by $D = \Delta z + \delta d$. This conversion is a standard procedure in direct force measurements.^{2,36} The resulting deflection versus distance profiles show that the deflection δd of the cantilever depends on the separation distance D from the solid surface. Comparison of the deflection profiles to the one acquired at $p_{\text{ext}} = 0$ mbar shows that the origin is

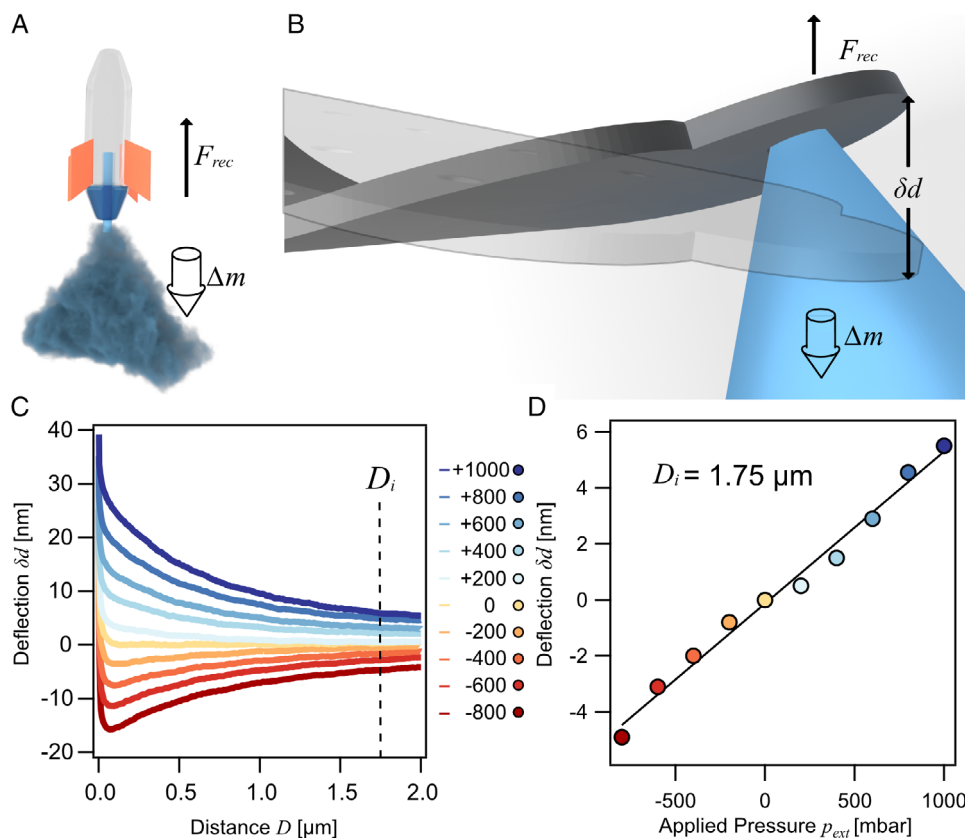


FIGURE 3 (A) Schematic representation of rocket propulsion. Due to the expulsion of mass Δm , a force is acting in the opposite direction. (B) Analogously, by the ejection of liquid through the aperture of a microchanneled cantilever, a recoil force can be observed that leads to the deflection of the cantilever. (C) Set of deflection versus distance curves for a microchanneled cantilever and a hard wall with different externally applied pressures. At short separation distances, the acting forces have been influenced by the underlying substrate, while at larger distances, practically only recoil to liquid ejection has been observed. Here, a cantilever with an aperture of $2 \mu m$ in diameter and a nominal spring constant of $2 N/m$ has been used. (D) Deflection versus applied pressure at a separation distance of $1.75 \mu m$ with a linear fit to the experimental data.

associated with hydrodynamic effects and not surface forces. At smaller separation distances between aperture and surface, the jet ejected from the cantilever's aperture, and the resulting impinging jet acts back on the cantilever, leading to an additional force contribution.⁷⁹ However, the absence of a dedicated nozzle on the cantilever (cf. Figure 2) leads to a strong reduction of this effect, which levels off rapidly with increasing separation. Similar type of interaction profiles between a FluidFM-cantilever ejecting a liquid jet and a solid surface have already been reported previously.^{17,75,80} For sufficiently large separation distances $D_i > 1.75 \mu m$, the interaction of the liquid jet with the solid surface can be neglected and thus is purely based on the recoil due to the ejected liquid.

Figure 3D shows all deflection values δd acquired at the separation distances of $1.75 \mu m$ (cf. Figure 3C) as function of the corresponding applied pressure p_{ext} . At this distance, one measures predominantly the deflection belonging to the recoil F_{rec} , which is given by Equation (3). The solid line in Figure 3D represents a linear fit forced through 0

and confirms the hypothesis of $F_{rec} \propto p_{ext}$ when taking into account $F_{rec} \propto \delta d$ according to Hooke's law (cf. Equation 3).

2.2 | Modeling the liquid flow inside a microchanneled cantilever

It is necessary to calculate the pressure Δp at the aperture (cf. Equation 3), as this pressure difference between the inside of the aperture and the bulk liquid does not correspond to the externally applied pressure p_{ext} due to the law of Hagen–Poiseuille. The latter accounts for the friction between the liquid and the walls of the cantilever microchannel. Thus, the parameters describing the flow through the channel, namely, dm/dt , Δp , and v_{ap} , must be approximated by a suitable model for the hydrodynamics inside the channel. For aqueous electrolyte solutions and the here-applied external pressures, the flow can be considered laminar and Newtonian.¹⁶ The total hydrodynamic resistance R of the microchanneled cantilever relates the

mass flow Q through the aperture while p_{ext} is applied:

$$Q = \frac{P_{\text{ext}}}{R} = \frac{P_{\text{ext}}}{R_{\text{ch}} + R_{\text{ap}}} \quad (4)$$

where R_{ch} and R_{ap} are the hydrodynamic resistances of a rectangular channel and a circular aperture, respectively. The resistances for these two geometries are^{64,81}

$$R_{\text{ch}} = \frac{12\eta l_{\text{ch}}}{w_{\text{ch}} h_{\text{ch}}^3} \left(1 - 0.63 \frac{h_{\text{ch}}}{w_{\text{ch}}} \right) \quad (5a)$$

and

$$R_{\text{ap}} = \frac{128\eta l_{\text{ap}}}{\pi d_{\text{ap}}^4} \quad (5b)$$

with l_{ch} as total channel length (cf. Supporting Information S1), w_{ch} as channel width, and h_{ch} as channel height, respectively. The geometry of the aperture is described by a cylindrical geometry using the cantilever's wall thickness l_{ap} and the aperture diameter d_{ap} . The dimensions of all microchanneled cantilevers used in this study have been compiled in Supporting Information S3. The viscosity η is the one of water at room temperature (25°C, $\eta = 0.001$ Pa s).

For a Newtonian fluid, the volume flow rate Q must be constant over the internal channel, and thus $Q = Q_{\text{ap}} = Q_{\text{ch}}$. The total flow rate Q through the channel can also be expressed as the product of flow velocity and cross-sectional area, that is, $Q = A_{\text{ap}} \cdot V_{\text{ap}} = A_{\text{ch}} \cdot V_{\text{ch}}$. Thus, the flow velocity at the aperture v_{ap} can be determined, as the cross-sectional area A_{ap} is known. The mass flow rate follows via the density of the fluid ρ and the area of the aperture A_{ap} :

$$\frac{dm}{dt} = \rho \cdot A_{\text{ap}} \cdot V_{\text{ap}} \quad (6)$$

The pressure Δp directly at the aperture cannot be retrieved by analytical methods. To determine Δp , we performed numerical simulations by the finite element method based on the program COMSOL. Comparable simulations have been carried out already in the past for microchanneled cantilevers.^{64,73,74} For these simulations, the internal geometry of the cantilever channels (cf. Supporting Information S3) has been fully implemented, including the pillars inside the channel (cf. Figure 2B and Supporting Information S1). Further details are given in the Supporting Information. Figure 4 shows the results of an exemplary simulation for a cantilever with an aperture diameter of 2 μm , an internal channel height of 1 μm , and an applied pressure of 1000 mbar, respectively. The pressure distributions inside the channel, at the aperture, and in the bulk liquid around the cantilever's aperture are rep-

resented by the color scale: inside the channel, only a small reduction of the pressure takes place, mainly due to friction between liquid and channel walls according to the law of Hagen–Poiseuille (cf. also simulation result in Supporting Information S7). The main pressure drop occurs around the aperture (cf. Figure 4A). The results of our simulation have been corroborated against COMSOL simulations of similar systems, and a very good agreement has been found.^{16,64,82} Further details are given in Supporting Information S2.

The externally applied pressure p_{ext} and Δp at the aperture can be placed in relation by $\Delta p = \chi p_{\text{ext}}$, with χ as pressure reduction coefficient. However, this coefficient must be determined for each cantilever geometry (cf. Supporting Information S3). The results for χ have been compiled in Figure 4B as a function of the aperture size and for different channel heights. As expected, χ decreases with increasing aperture size d_{ap} as larger apertures act less effectively as a nozzle. On the other hand, with increasing channel height h_{ch} , the hydrodynamic focussing at the aperture exit increases and larger values for χ are found for the same aperture diameter. Larger data points represent cantilever geometries that are commercially available and have been experimentally addressed in the following sections.

2.3 | Implementing the hydrodynamic calibration method for the (inverse) optical lever sensitivity

Having a model for the liquid flow in and out of the microchannel allows to calculate the acting recoil force F_{rec} solely based on the geometrical dimensions of the cantilever channel and the externally applied pressure p_{ext} . The dimensions of the internal channel and the aperture l_{ch} , w_{ch} , h_{ch} , and d_{ap} remain constant throughout the production process and only small variation is found. The nominal values provide, to our experience, a very good approximation (cf. insets in Figure 4B and Table in Supporting Information S3). However, d_{ap} shows significant variation in the production process, but can be determined easily post-measurement by microscopic techniques (e.g., SEM). Hence, with the tabulated values of χ and Equations (3)–(6), one can calculate F_{rec} for a given pressure p_{ext} . With the cantilever's spring constant k_{c} , one can calculate the expected deflection δd via Equation (2) from F_{rec} . Therefore, measuring ΔU as a function of p_{ext} provides a direct way to determine InvOLS via Equation (1). In the following, we discuss two possible procedures to carry out this determination: In the first procedure, an external pressure p_{ext} is applied in a defined number of steps and for specified time intervals. The response of the

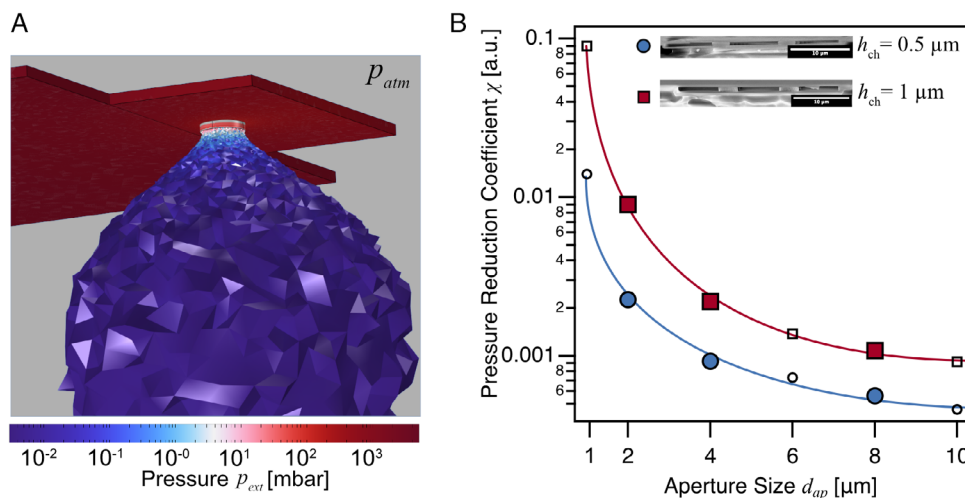


FIGURE 4 (A) Finite element analysis by COMSOL of the fluid flow through microchanneled cantilevers. Based on this simulation, which includes the entire geometry of the internal channel, the pressure Δp at the aperture can be determined for an externally applied p_{ext} . Thereby, the pressure reduction coefficient χ according to $\Delta p = \chi \cdot p_{ext}$ has been calculated. (B) Compilation of χ -values as function of aperture size d_{ap} , which has by far the largest influence on χ . Results for two different channel heights (cf. inset) are shown (circles and squares). The large symbols represent microchanneled cantilevers that are commercially available and that have been tested here.

photodetector signal, that is, $\Delta U(p_{ext})$ is measured and averaged for each pressure pulse. In the following, we refer to this method as “pulse procedure.” The data evaluation for this procedure has been performed by a custom-written procedure in IgorPro, which detects the different steps and then averages a suitable number of points, depending on the sampling rate, on both levels of the step. Additionally, the pressure difference for these steps is determined from the data of the pressure sensor. In the second, alternative procedure, a continuous pressure ramp from low to high p_{ext} values is applied. The corresponding voltage response $\Delta U(p_{ext})$ has been measured for each single data point of the pressure ramp. We refer to this approach as “ramp procedure.” It should be emphasized that both procedures are completely contact-free. The noise level for both calibration procedures depends largely on the pressure controller and the vibration transmitted through the tubing. Moreover, the general acoustic and vibrational isolation of the setup is of great importance.

Figure 5A shows the results of the “pulse procedure” for a microchanneled cantilever with a nominal aperture $d_{ap} = 2 \mu\text{m}$ and a spring constant $k_c = 2.4 \text{ N/m}$ as determined by the method of Cleveland et al.²⁷ In Figure 5A, the applied pressure pulses (bottom) and the resulting photodiode readouts ΔU (top) are shown. These measurements have been performed at separation distances of greater than $10 \mu\text{m}$. For each pressure pulse, the response of the cantilever took place very fast, and an equilibrium deflection is practically reached for the entire length of the pulse. The first data points result from an overshoot of the pressure controller PID. The scattering of the deflection data results most likely from vibrations due to the pressure con-

troller and its tubing, as well as from the thermal excitation of the cantilever. Figure 5B plots ΔU (as measured) versus δd (as determined from p_{ext}) for the averages on the different steps. The resulting data points for the different pressure pulses must follow, according to Equation (1), a line whose slope is the InvOLS. Indeed, to a good level of agreement, the data follow linear behavior, and the slope of the linear fit leads to an InvOLS of 59.08 nm/V , which is in reasonable agreement with an InvOLS of 49.00 nm/V , as determined beforehand by the conventional method.

Figure 5C,D shows the results for the “ramp procedure” for the same cantilever as in Figure 5A,B. These data were acquired shortly ($<5 \text{ min}$) after those acquired by the “pulse procedure.” For the ramp method, the pressure p_{ext} has been increased linearly, and the resulting photodetector response has been acquired ΔU (cf. Figure 5C). Following the same conversion of p_{ext} to δd , also here a linear dependence of ΔU on δd has been observed. For the ramp method, we find under comparable conditions a sensitivity of $\text{InvOLS} = 56.95 \text{ nm/V}$, which agrees very well with the values obtained by the step procedure. Both methods thus lead to comparable values for InvOLS. However, the measurement by the ramp procedure required less than 30 s .

2.4 | Hydrodynamic recoil versus constant compliance calibration on substrate

In order to evaluate the performance of the here-developed calibration method, it has been compared with the

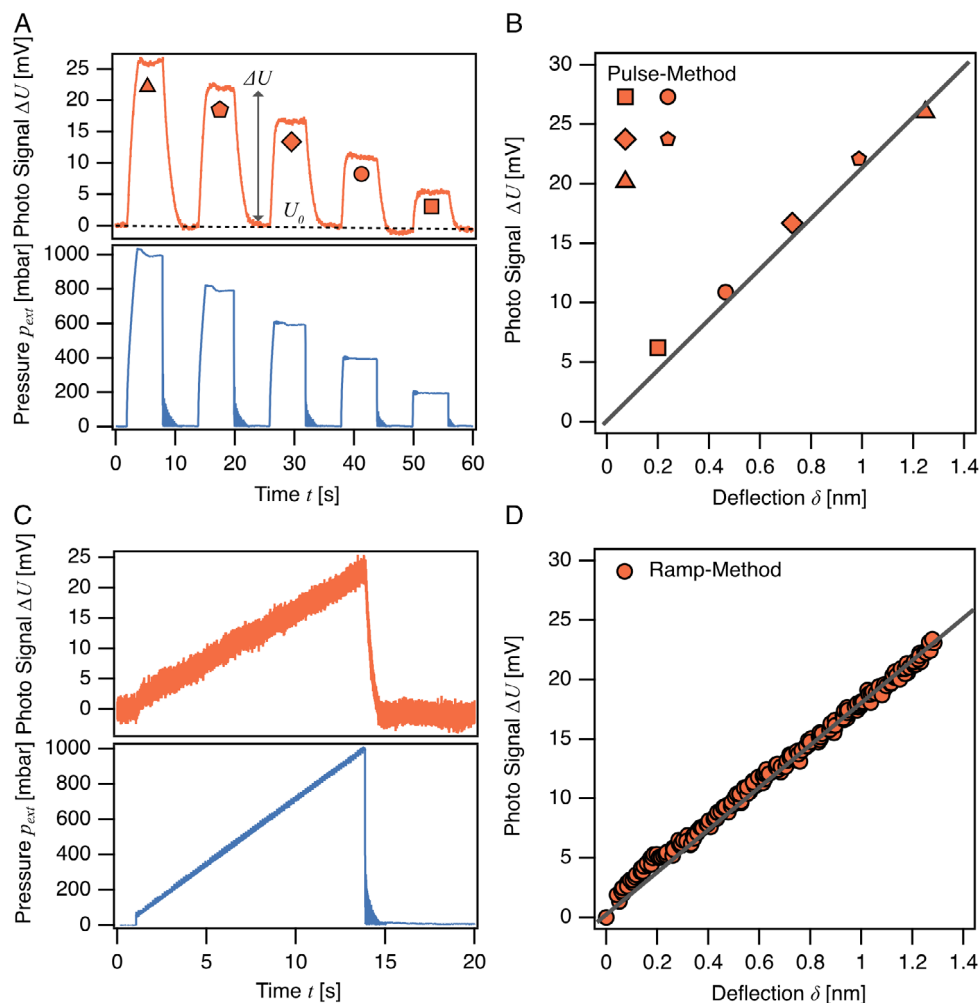


FIGURE 5 Two different procedures for the calibration of InvOLS by the hydrodynamic recoil force for the same microchanneled cantilever (nominal aperture of $2\ \mu\text{m}$ and nominal spring constant of $2\ \text{N/m}$) under identical experimental conditions. (A and B) “Pulse procedure,” which is based on short (e.g., 6 s) pressure pulses and (C and D) “ramp procedure.” (A) The cantilever response in terms of the resulting photodiode signal is detected for each of the pulses, and an overall, averaged response in terms of ΔU is given for each pressure p_{ext} assigned to the different pulses. Here, resulting pulses are represented by different symbols. (C and D) “Ramp procedure,” is based on continuously ramping up the pressure from very low to high values, while recording the photodiode signal. ΔU is then determined as a line fit over the whole pressure range. Calculation of InvOLS leads to 59.08 and 56.95 nm/V for the “pulse procedure” and the “ramp procedure,” respectively.

classical method for determining InvOLS, which is based on ramping the cantilever against a non-deformable surface and fitting the resulting constant compliance region. We performed two different sets of experiments: In the first set of experiments, we changed the values for InvOLS for one microchanneled cantilever by changing the position of the laser spot on the FluidFM-cantilever, while the cantilever and the rest of the experimental setup remained unchanged. Due to the importance of the laser position on the cantilever, this approach allows a highly defined variation of the optical lever sensitivity while practically eliminating all other parameter changes. In a second set of experiments, we utilized several microchanneled-cantilevers ($n = 12$) of different types and geometries

(cf. Supporting Information S3), thereby varying the parameters A_{ap} and h_{ch} . By this set of experiments, we could evaluate how the differences in cantilever structure influenced the accuracy of the new calibration approach.

Figure 6A shows the results for the first set of experiments varying the spot position. A FluidFM-cantilever with a nominal aperture of $2\ \mu\text{m}$ in diameter and a nominal $2\ \text{N/m}$ spring constant has been used. It is well known that the laser’s position on the cantilever strongly influences the InvOLS.^{83,84} This change should have an equal influence on both optical lever sensitivity calibration methods, that is, the classical, mechanic approach and the novel, hydrodynamic one. The independently determined InvOLS values for both methods have been

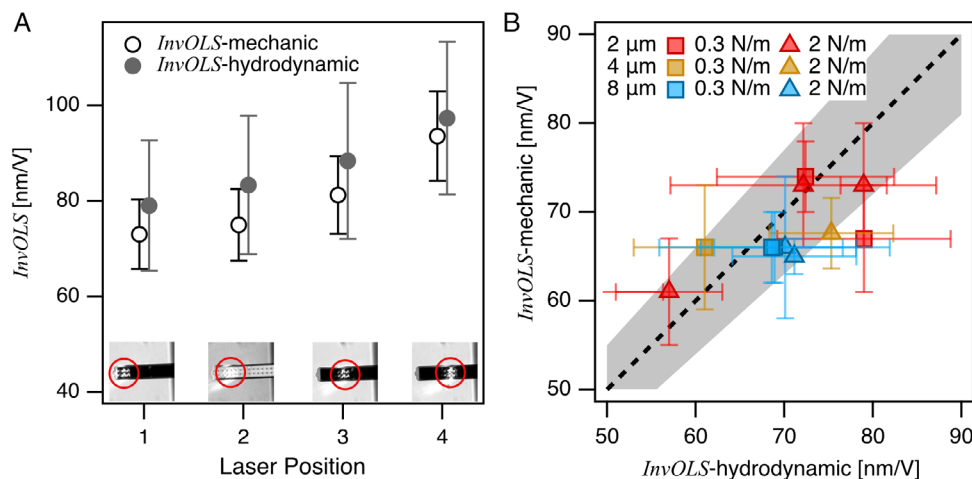


FIGURE 6 Comparing the calibration of InvOLS by the here-developed hydrodynamic method with the classical mechanical method. (A) Variation of InvOLS by shifting the position of the laser spot on the cantilever (cf. insets of the graph). The error bars result from different measurements ($n = 40$ ramps). (B) Scatter plot of the experimentally determined InvOLS-values for the two different methods. The data points represent different microchanneled cantilevers varying aperture diameter and channel height (cf. figure legend). The solid line represents a linear fit to the data. The resulting slope was 0.94, which has to be compared to 1.0 for an ideal match between both methods. The grey area indicates the error distribution of the linear fit.

plotted in Figure 6A for the different laser spot positions. For the latter method, we did utilize the ramp procedure. The error bars shown result from at least 40 ramps. The resulting error of 10% and 15%, respectively, approximately corresponds to the error stated in the literature for measurements of the optical lever sensitivity.³³

Figure 6B shows how for a large selection of different types of FluidFM-cantilevers, the here-developed hydrodynamic method compares to the “classical” InvOLS determination by mechanical response on a non-deformable substrate. We compared both methods for all types of cantilevers listed in the Supporting Information, which corresponds to practically all FluidFM-cantilevers commercially available with an aperture greater than 1 μm. We attribute the scattering of the data in Figure 5B primarily to production variations in the aperture size and variations as well as debris in the channel. Especially, the former parameter is of great significance for calculating χ . However, it should be pointed out that the main deviations originate mostly from only two cantilevers, which show deviations between both methods larger than 10% but smaller than 20%.

3 | CONCLUSION

The here-presented approach for calibration of the InvOLS leads not only to reliable results but is extremely fast, does not require contact with any surface, and can be integrated easily into any workflow. We compiled the necessary values for χ in the Supporting Information for use by other

researchers. Additionally, only calibration of the spring constant k_c is required in the here-presented method (e.g., by the Cleveland method).

In particular, for automatized measurements this new approach for the InvOLS-calibration can be easily implemented and will allow to determine InvOLS between single measurement series. As fluidic force microscopy is increasingly utilized to characterize cell–substrate interactions,⁵⁶ nano-structuring,^{58,59} and is utilized for sampling cells or cell organelles,⁵⁷ the here-presented approach might be extremely useful due to the fact that the optical lever sensitivity can be determined in short time, that is, seconds, and most of all contact free. Thereby corrections for drift and prevention for contamination are easily implementable in the workflow, in particular for robotic approaches.^{21,42,43}

4 | MATERIALS AND METHODS

4.1 | Materials

Milli-Q grade deionized water, with a resistivity of greater than 18.2 MΩ at 25°C, was used for all measurements. For filling the measuring cell, the water was filtered using syringe filters with a pore size of 0.22 μm (Carl Roth GmbH & Co KG). As substrates, circular glass disks with a diameter of 25 mm (Irlbacher Blickpunkt Glas GmbH) have been used, which have been cleaned by plasma treatment before use (Zepto, Diener Electronics).

4.2 | Microchanneled cantilevers

Microchanneled cantilevers with different channel heights and aperture diameters have been purchased from Cytosurge AG. For all microchanneled cantilevers, the width of the channel was $27 \pm 3 \mu\text{m}$ and length $1100 \pm 110 \mu\text{m}$.⁶⁵ The channel height was $0.95 \pm 0.05 \mu\text{m}$ for cantilevers with 2 N/m and $0.5 \pm 0.05 \mu\text{m}$ for 0.3 N/m, respectively. Nominal aperture sizes of 2, 4, and 8 μm have been used.

4.3 | Scanning electron microscopy

SEM of the cantilevers has been carried out with a TM3030 (Hitachi). The SEM has been operated in vacuum mode with an acceleration voltage of 15 kV. No pretreatment in terms of coating was necessary.

4.4 | Finite element simulations

Finite element simulations were calculated by Comsol Multiphysics 5.6 (Comsol Multiphysics GmbH). The model used was the laminar flow model, a standard model of Comsol under the assumptions of no-slip boundary and laminar flow over the whole geometry. The simulation was carried out with a 3D model of the fluid-filled part of the cantilever. The pressure at the aperture was determined by calculating the mean value over the whole volume of the aperture.

4.5 | Fluidic force microscopy

All experiments have been performed with a commercial AFM-System (FlexAFM V5 equipped with a SLD and a C3000 controller, Nanosurf AG), which has been mounted on an inverted optical microscope (Axio Observer Z1, Carl Zeiss AG). The AFM and optical microscope have been placed on an active damping system (Halcyonics Variobasic, Accurion GmbH), which was set up in an acoustic enclosure (Accurion GmbH). A fluid cell in which circular glass slides could be mounted (Asylum Research, Oxford Instruments) has been used throughout the experiments presented here. A commercial microfluidic pressure controller (Cytosurge AG) was used to apply an external pressure to the microchanneled cantilevers.

Before the experiments, the microchanneled cantilevers were filled with more than 30 μL of Milli-Q water by means of a syringe coupled to a filter. The cantilever was then connected via a microfluidic connector to the pressure controller (cf. Supporting Information S4). By applying a pressure of 300 mbar, the microchannel was

filled. The process of filling the microchannel was monitored by optical microscopy. The presence of a small liquid drop at the aperture confirms completion of the filling process and the cantilever was immersed in the liquid cell, which had been filled with water beforehand. The InvOLS was determined conventionally by performing direct force measurements against the glass substrate. For calibration, z -scan of 1 μm was used with a setpoint of 300 mV and a ramping rate of 1 Hz. The spring constant of the cantilevers has been calibrated by means of the added-mass method in air (Cleveland method).²⁷ The resonance frequency was recorded for at least five attached tungsten particles for each cantilever. The individual diameter for each of the tungsten spheres, as well as its position on the cantilever, has been determined by optical microscopy.⁸⁵

4.6 | Implementation of the hydrodynamic InvOLS calibration

Two procedures for the contactless calibration of microchanneled cantilevers were implemented: (i) pulse procedure, and (ii) ramp procedure. For both procedures, the cantilever was removed at least 30 μm from the glass surface. The z -movement was paused for the duration of the calibration procedures. For the pulse procedure (i), defined pressure pulses in the range of +200 to +1000 mbar were applied for 6 s while recording the resulting deflection of the cantilever. The step is performed using a home-written procedure in IgorPro, which detects the step and then averages a suitable number of points, depending on the sampling rate, on both levels of the step, subsequently, the step height is determined. For the ramp procedure, the applied pressure was gradually increased (from +50 to +1000 mbar) in 5-mbar steps, with a time increment shorter than the response time of the cantilever, making the deflection response continuous. For the ramp procedure (ii), the externally applied pressure and the resulting photodiode signal were captured via the analog inputs of the C3000 controller. For evaluation of both procedures, custom programs written in the software Igor Pro 6.37 (Wavemetrics, Inc.) have been developed.

ACKNOWLEDGMENTS

This study was funded by the Deutsche Forschungsgemeinschaft (DFG, German Research Foundation): 391977956-SFB 1357/B01, 491183248. Funded by the Open Access Publishing Fund of the University of Bayreuth. The authors also acknowledge support by the Elite Network of Bavaria (ENB) through the study program “Macromolecular Science”. The authors also acknowledge support by the University of Bayreuth Graduate School.

CONFLICT OF INTEREST STATEMENT

The authors declare no conflict of interest.

ORCID

Sebastian Sittl  <https://orcid.org/0009-0003-4996-5380>

Nicolas Helfricht  <https://orcid.org/0000-0002-5839-9670>

Georg Papastavrou  <https://orcid.org/0000-0002-5870-6693>

REFERENCES

- G. Binnig, C. F. Quate, C. Gerber, *Phys. Rev. Lett.* **1986**, *56*, 930.
- H.-J. Butt, B. Cappella, M. Kappl, *Surf. Sci. Rep.* **2005**, *59*, 1.
- H.-J. Butt, R. Berger, E. Bonaccorso, Y. Chen, J. Wang, *Adv. Colloid Interface Sci.* **2007**, *133*, 91.
- M. Krieg, G. Fläschner, D. Alsteens, B. M. Gaub, W. H. Roos, G. J. L. Wuite, H. E. Gaub, C. Gerber, Y. F. Dufrêne, D. J. Müller, *Nat. Rev. Phys.* **2019**, *1*, 41.
- D. Alsteens, H. E. Gaub, R. Newton, M. Pfreundschuh, C. Gerber, D. J. Müller, *Nat. Rev. Mater.* **2017**, *2*, 1.
- Y. F. Dufrêne, T. Ando, R. Garcia, D. Alsteens, D. Martinez-Martin, A. Engel, C. Gerber, D. J. Müller, *Nat. Nanotechnol.* **2017**, *12*, 295.
- K. Bian, C. Gerber, A. J. Heinrich, D. J. Müller, S. Scheuring, Y. Jiang, *Nat. Rev. Methods Primers* **2021**, *1*, 36.
- A. L. Weisenhorn, P. K. Hansma, T. R. Albrecht, C. F. Quate, *Appl. Phys. Lett.* **1989**, *54*, 2651.
- W. A. Ducker, T. J. Senden, R. M. Pashley, *Nature* **1991**, *353*, 239.
- H.-J. Butt, *Biophys. J.* **1991**, *60*, 1438.
- S. Rentsch, R. Pericet-Camara, G. Papastavrou, M. Borkovec, *Phys. Chem. Chem. Phys.* **2006**, *8*, 2531.
- J. Helenius, C.-P. Heisenberg, H. E. Gaub, D. J. Müller, *J. Cell Sci.* **2008**, *121*, 1785.
- J. Friedrichs, J. Helenius, D. J. Müller, *Nat. Protocols* **2010**, *5*, 1353.
- N. Helfricht, E. Doblhofer, V. Bieber, P. Lommes, V. Sieber, T. Scheibel, G. Papastavrou, *Soft Matter* **2017**, *13*, 578.
- A. Meister, M. Gabi, P. Behr, P. Studer, J. Voeroes, P. Niedermann, J. Bitterli, J. Polesel-Maris, M. Liley, H. Heinzlmann, T. Zambelli, *Nano Lett.* **2009**, *9*, 2501.
- P. Dörig, D. Ossola, A. M. Truong, M. Graf, F. Stauffer, J. Vörös, T. Zambelli, *Biophys. J.* **2013**, *105*, 463.
- N. Helfricht, A. Mark, L. Dorwling-Carter, L. Dorwling-Carter, T. Zambelli, G. Papastavrou, *Nanoscale* **2017**, *9*, 9491.
- A. Mark, N. Helfricht, A. Rauh, M. Karg, G. Papastavrou, *Small* **2019**, *15*, 1902976.
- P. Dörig, P. Stiefel, P. Behr, E. Sarajlic, D. Bijl, M. Gabi, J. Voeroes, J. A. Vorholt, T. Zambelli, *Appl. Phys. Lett.* **2010**, *97*, 023701.
- C. G. Gäbelein, Q. Feng, E. Sarajlic, T. Zambelli, O. Guillaume-Gentil, B. Kornmann, J. A. Vorholt, *PLoS Biol.* **2022**, *20*, e3001576.
- M. Sztilkovichs, T. Gerecsei, B. Peter, A. Saftics, S. Kurunczi, I. Szekacs, B. Szabo, R. Horvath, *Sci. Rep.* **2020**, *10*, 61.
- A. Sancho, I. Vandersmissen, S. Craps, A. Luttun, J. Groll, *Sci. Rep.* **2017**, *7*, 461.
- A. Sancho, M. B. Taskin, L. Wistlich, P. Stahlhut, K. Wittmann, A. Rossi, J. Groll, *ACS Biomater. Sci. Eng.* **2022**, *8*, 649.
- O. Guillaume-Gentil, C. G. Gäbelein, S. Schmieder, V. Martinez, T. Zambelli, M. Künzler, J. A. Vorholt, *Commun. Biol.* **2022**, *5*, 180.
- O. Guillaume-Gentil, R. V. Grindberg, R. Kooger, L. Dorwling-Carter, V. Martinez, D. Ossola, M. Pilhofer, T. Zambelli, J. A. Vorholt, *Cell* **2016**, *166*, 506.
- J. L. Hutter, J. Bechhoefer, *Rev. Sci. Instrum.* **1993**, *64*, 1868.
- J. P. Cleveland, S. Manne, D. Bocek, P. K. Hansma, *Rev. Sci. Instrum.* **1993**, *64*, 403.
- J. E. Sader, I. Larson, P. Mulvaney, L. R. White, *Rev. Sci. Instrum.* **1995**, *66*, 3789.
- J. E. Sader, J. W. M. Chon, P. Mulvaney, *Rev. Sci. Instrum.* **1999**, *70*, 3967.
- G. A. Matei, E. J. Thoreson, J. R. Pratt, D. B. Newell, N. A. Burnham, *Rev. Sci. Instrum.* **2006**, *77*, 083703.
- J. te Riet, A. J. Katan, C. Rankl, S. W. Stahl, A. M. van Buul, I. Y. Phang, A. Gomez-Casado, P. Schon, J. W. Gerritsen, A. Cambi, A. E. Rowan, G. J. Vancso, P. Jonkheijm, J. Huskens, T. H. Oosterkamp, H. Gaub, P. Hinterdorfer, C. G. Figdor, S. Speller, *Ultramicroscopy* **2011**, *111*, 1659.
- Á. G. Nagy, J. Kámán, R. Horváth, A. Bonyár, *Sci. Rep.* **2019**, *9*, 10287.
- M. J. Higgins, R. Proksch, J. E. Sader, M. Polcik, S. Mc Endoo, J. P. Cleveland, S. P. Jarvis, *Rev. Sci. Instrum.* **2006**, *77*, 013701.
- G. Meyer, N. M. Amer, *Appl. Phys. Lett.* **1988**, *53*, 1045.
- D. T. Edwards, T. T. Perkins, *J. Struct. Biol.* **2017**, *197*, 13.
- T. J. Senden, *Curr. Opin. Colloid Interface Sci.* **2001**, *6*, 95.
- M. Allegrini, C. Ascoli, P. Baschieri, F. Dinelli, C. Frediani, A. Lio, T. Mariani, *Ultramicroscopy* **1992**, *42*, 371.
- J. Kámán, R. Huszánk, A. Bonyár, *Micron* **2019**, *125*, 102717.
- C. T. Gibson, B. L. Weeks, J. R. I. Lee, C. Abell, T. Rayment, *Rev. Sci. Instrum.* **2001**, *72*, 2340.
- T. Witko, Z. Baster, Z. Rajfur, K. Sofińska, J. Barbasz, *Sci. Rep.* **2021**, *11*, 209.
- V. S. J. Craig, C. Neto, *Langmuir* **2001**, *17*, 6018.
- A. Saftics, B. Türk, A. Sulyok, N. Nagy, T. Gerecsei, I. Szekacs, S. Kurunczi, R. Horvath, *Langmuir* **2019**, *35*, 2412.
- Á. G. Nagy, N. Kanyó, A. Vörös, I. Székács, A. Bonyár, R. Horvath, *Sci. Rep.* **2022**, *12*, 7747.
- N. P. D'Costa, J. H. Hoh, *Rev. Sci. Instrum.* **1995**, *66*, 5096.
- L. Y. Beaulieu, M. Godin, O. Laroche, V. Tabard-Cossa, P. Grütter, *Ultramicroscopy* **2007**, *107*, 422.
- A. Weber, B. Zbiral, J. Iturri, R. Benitez, J. L. Toca-Herrera, *Microsc. Res. Tech.* **2021**, *84*, 1078.
- A. Weber, J. Iturri, R. Benitez, J. L. Toca-Herrera, *Microsc. Res. Tech.* **2019**, *82*, 1392.
- J. Domke, M. Radmacher, *Langmuir* **1998**, *14*, 3320.
- H. Schillers, C. Rianna, J. Schäpe, T. Luque, H. Doschke, M. Wälte, J. J. Uriarte, N. Campillo, G. P. A. Michanetzis, J. Bobrowska, A. Dumitru, E. T. Herruzo, S. Bovio, P. Parot, M. Galluzzi, A. Podestà, L. Puricelli, S. Scheuring, Y. Missirlis, R. Garcia, M. Odorico, J.-M. Teulon, F. Lafont, M. Lekka, F. Rico, A. Rigato, J.-L. Pellequer, H. Oberleithner, D. Navajas, M. Radmacher, *Sci. Rep.* **2017**, *7*, 265.
- C. T. Gibson, G. S. Watson, S. Myhra, *Scanning* **2006**, *19*, 564.
- J. P. Best, J. Cui, M. Müllner, F. Caruso, *Langmuir* **2013**, *29*, 9824.
- R. Buzio, A. Bosca, S. Krol, D. Marchetto, S. Valeri, U. Valbusa, *Langmuir* **2007**, *23*, 9293.

53. O. Guillaume-Gentil, E. Potthoff, D. Ossola, C. M. Franz, T. Zambelli, J. A. Vorholt, *Trends Biotechnol.* **2014**, *32*, 381.
54. M. Li, L. Liu, T. Zambelli, *Nano Res.* **2022**, *15*, 773.
55. P. Saha, T. Duanis-Assaf, M. Rechtes, *Adv. Mat. Interfaces* **2020**, *7*, 2001115.
56. L. Angeloni, B. Popa, M. Nouri-Goushki, M. Minneboo, A. A. Zadpoor, M. K. Ghatkesar, L. E. Fratila-Apachitei, *Small* **2023**, *19*, 2204662.
57. P. Actis, *Small Methods* **2018**, *2*, 1700300.
58. N. Helfricht, A. Mark, M. Behr, A. Bernet, H.-W. Schmidt, G. Papastavrou, *Small* **2017**, *13*, 1700962.
59. E. Berganza, E. Boltynjuk, G. Mathew, F. F. Vallejo, R. Gröger, T. Scherer, S. Sekula-Neuner, M. Hirtz, *Small* **2023**, *19*, 2205590.
60. D. Ossola, L. Dorwling-Carter, H. Dermutz, P. Behr, J. Vörös, T. Zambelli, *Phys. Rev. Lett.* **2015**, *115*, 238103.
61. L. Dorwling-Carter, M. Aramesh, C. Forró, R. F. Tiefenauer, I. Shorubalko, J. Vörös, T. Zambelli, *J. Appl. Phys.* **2018**, *124*, 174902.
62. L. Hirt, A. Reiser, R. Spolenak, T. Zambelli, *Adv. Mater.* **2017**, *29*, 1604211.
63. J. Ko, N. B. Fredj, R. E. Adhawiyah, J. Lee, *J. Mech. Sci. Technol.* **2023**, *37*, 887.
64. T. Zambelli, J. Aebbersold, M. Behr, P. Han, H. Hirt, L. Martinez, V. Guillaume-Gentil, O. Vörös, *Open-Space Microfluidics: Concepts, Implementations, Applications*, Wiley-VCH Verlag, Weinheim, Germany **2018**.
65. A. Mark, N. Helfricht, A. Rauh, J. Xue, P. Knödler, T. Schumacher, M. Karg, B. Du, M. Lippitz, G. Papastavrou, *Sci. Rep.* **2019**, *9*, 20294.
66. G. Göring, P.-I. Dietrich, M. Blaicher, S. Sharma, J. G. Korvink, T. Schimmel, C. Koos, H. Hölscher, *Appl. Phys. Lett.* **2016**, *109*, 063101.
67. A. Gaitas, R. Malhotra, K. Pienta, *Appl. Phys. Lett.* **2013**, *103*, 123702.
68. A. Gaitas, R. W. Hower, *J. Micro/Nanotech. MEMS MOEMS* **2014**, *13*, 030501.
69. C.-C. Chien, J. Jiang, B. Gong, T. Li, A. Gaitas, *Meas. Sci. Technol.* **2022**, *33*, 095009.
70. S. Deladi, N. R. Tas, J. W. Berenschot, G. J. M. Krijnen, M. J. de Boer, J. H. de Boer, M. Peter, M. C. Elwenspoek, *Appl. Phys. Lett.* **2004**, *85*, 5361.
71. R. van Oorschot, H. H. Perez Garza, R. J. S. Derks, U. Staufer, M. K. Ghatkesar, *EPJ Tech Instrum* **2015**, *2*, 4.
72. H. Garza, M. Ghatkesar, S. Basak, P. Löthman, U. Staufer, *Micromachines* **2015**, *6*, 600.
73. D. Ossola, P. Dörig, J. Vörös, T. Zambelli, M. Vassalli, *Nanotechnology* **2016**, *27*, 415502.
74. A. Gabor Nagy, N. Pap, R. Horvath, A. Bonyar, *IEEE, 44th International Spring Seminar on Electronics Technology (ISSE)*, Bautzen, **2021**.
75. R. R. Grüter, B. Dielacher, L. Hirt, J. Vörös, T. Zambelli, *Nanotechnology* **2015**, *26*, 175301.
76. U. Walter, *Astronautics*. p. 1–35, Springer International Publishing, Cham **2018**.
77. J.-B. Bao, D. Jed Harrison, *AIChE J.* **2006**, *52*, 75.
78. O. Geschke, H. Klank P. Telleman, *Microsystem Engineering of Lab-on-a-Chip Devices*, Wiley-VCH, Weinheim **2004**.
79. B. Hu, H. Wang, J. Liu, Y. Zhu, C. Wang, J. Ge, Y. Zhang, *J. Marine Sci. Eng.* **2022**, *10*, 228.
80. D. Ossola, *PhD Thesis*, ETH Zürich **2014**.
81. S. Hardt F. Schönfeld, *Microfluidic Technologies for Miniaturized Analysis Systems*, Springer US, Boston, MA **2007**.
82. P. Dörig, *PhD Thesis*, ETH Zürich, **2013**.
83. Z. Liu, Y. Jeong, C.-H. Menq, *Rev. Sci. Instrum.* **2013**, *84*, 023703.
84. J. Putnam, M. Damircheli, B. Eslami, *J. Multibody Dyn.* **2020**, *234*, 675.
85. R. Proksch, T. E. Schaffer, J. P. Cleveland, R. C. Callahan, M. B. Viani, *Nanotechnology* **2004**, *15*, 1344.

SUPPORTING INFORMATION

Additional supporting information can be found online in the Supporting Information section at the end of this article.

How to cite this article: S. Sittl, N. Helfricht, G. Papastavrou, *VIEW*. **2024**, *5*, 20230063.
<https://doi.org/10.1002/VIW.20230063>